

SurfelGAN: Synthesizing Realistic Sensor Data for Autonomous Driving

Zhenpei Yang^{1*}, Yuning Chai², Dragomir Anguelov², Yin Zhou², Pei Sun²,
Dumitru Erhan³, Sean Rafferty², Henrik Kretzschmar²
¹UT Austin, ²Waymo, ³Google Brain

Abstract

Autonomous driving system development is critically dependent on the ability to replay complex and diverse traffic scenarios in simulation. In such scenarios, the ability to accurately simulate the vehicle sensors such as cameras, lidar or radar is hugely helpful. However, current sensor simulators leverage gaming engines such as Unreal or Unity, requiring manual creation of environments, objects, and material properties. Such approaches have limited scalability and fail to produce realistic approximations of camera, lidar, and radar data without significant additional work.

In this paper, we present a simple yet effective approach to generate realistic scenario sensor data, based only on a limited amount of lidar and camera data collected by an autonomous vehicle. Our approach uses texture-mapped surfels to efficiently reconstruct the scene from an initial vehicle pass or set of passes, preserving rich information about object 3D geometry and appearance, as well as the scene conditions. We then leverage a SurfelGAN network to reconstruct realistic camera images for novel positions and orientations of the self-driving vehicle and moving objects in the scene. We demonstrate our approach on the Waymo Open Dataset and show that it can synthesize realistic camera data for simulated scenarios. We also create a novel dataset that contains cases in which two self-driving vehicles observe the same scene at the same time. We use this dataset to provide additional evaluation and demonstrate the usefulness of our SurfelGAN model.

1. Introduction

Recent advances in deep learning have inspired breakthroughs in multiple areas related to autonomous driving such as perception [16, 27], prediction [5, 7] and planning [13]. These recent trends only underscore the increasingly significant role of data-driven system development. One aspect is that deep learning networks benefit from large training datasets. Another is that autonomous driving sys-

tem evaluation requires the ability to realistically replay a large set of diverse and complex scenarios in simulation capturing sensor properties, seasons, time of day, and weather. Developing simulators that support the levels of realism required for autonomous system evaluation is a challenging task. There are many ways to design simulators, including simulating *mid-level* object representations [5, 12]. However, mid-level representations omit subtle perceptual cues that are important for scene understanding, such as pedestrian gestures and blinking lights on vehicles. Furthermore, as end-to-end models that combine perception, prediction, and sometimes even control become an increasingly more popular direction of research, we are faced with the need to faithfully simulate the sensor data, which is the input to such models during scenario replay.

Frameworks for autonomous driving that support realistic sensor simulation are traditionally built on top of gaming engines such as Unreal or Unity [12]. The environment and its object models are created and arranged manually, to approximate real-world scenes of interest. In order to enable realistic LiDAR and radar modeling, material properties often need to be manually specified as well. The overall process is time-consuming and not scalable. Furthermore, simple ray-casting or ray-tracing techniques are often insufficient to generate realistic camera, LiDAR, or radar data for a specific self-driving system, and additional work is required to adapt the simulated sensor statistics to the real sensors.

In this work, we propose a simple yet effective data-driven approach for creating realistic scenario sensor data. Our approach relies on camera and LiDAR data collected in a single pass, or several passes, of an autonomous vehicle through a scene of interest. We use this data to reconstruct the scene using a texture-mapped surfel representation. This representation is simple and computationally efficient to create and preserves rich information about the 3D geometry, semantics, and appearance of all objects in the scene. Given the surfel reconstruction, we can render the scene for novel poses of the self-driving vehicle (SDV) and the other scenario agents. The rendered reconstruction for these novel views may have some missing parts due to occlusion differences between the initial and the new configuration. It can

*Work done as an intern at Waymo. Correspondence: yzp@utexas.edu

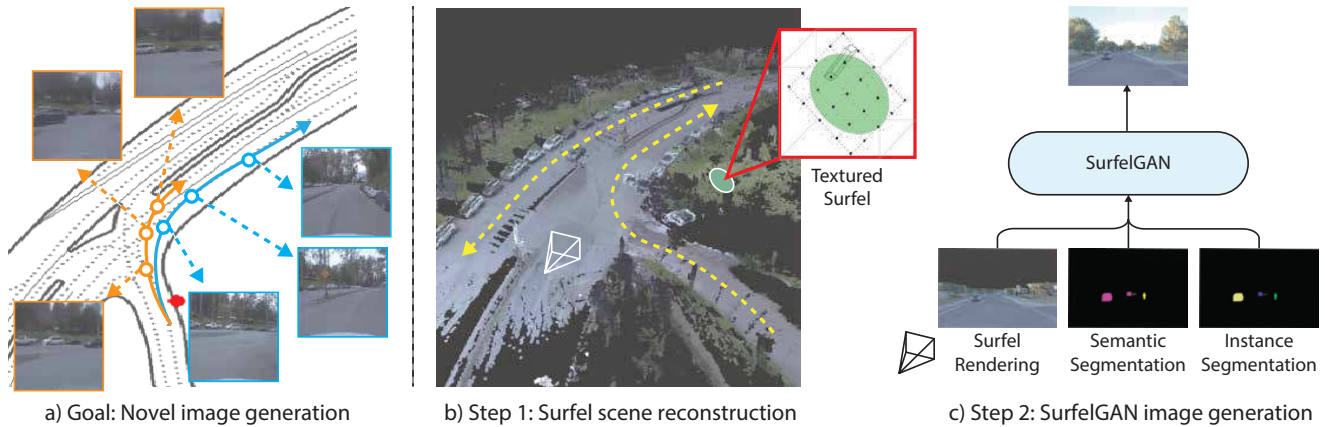


Figure 1. **Overview of our proposed system.** a) The goal of this work is the generation of camera images for autonomous driving simulation. When provided with a novel trajectory of the self-driving vehicle in simulation, the system generates realistic visual sensor data that is useful for downstream modules such as an object detector, a behavior predictor, or a motion planner. At a high level, the method consists of two steps: b) First, we scan the target environment and reconstruct a scene consisting of rich textured surfels. c) Surfels are rendered at the camera pose of the novel trajectory, alongside semantic and instance segmentation masks. Through a GAN [15], we generate realistically looking camera images.

also have visual quality artifacts due to the limited fidelity of the surfel reconstruction. We address this gap by applying a GAN network [15] to the rendered surfel views to produce the final high-quality image reconstructions. An overview of our proposed system is illustrated in Fig. 1.

Our work makes the following contributions: 1) We describe a pipeline that builds a detailed reconstruction of a dynamic scene from real-world sensor data. This representation allows us to render novel views in the scene, corresponding to deviations of the SDV and the other agents in the environment from their initially captured trajectories (Sec. 3.1). 2) We propose a GAN architecture that takes in the rendered surfel views and synthesizes images with quality and statistics approaching that of real images (Tab. 1) 3) We build the first dataset for reliably evaluating the task of novel view synthesis for autonomous driving, which contains cases in which two self-driving vehicles observe the same scene at the same time. We use this dataset to provide additional evaluation and demonstrate the usefulness of our SurfelGAN model.

2. Related Work

Simulated Environment for Learning Agent. There have been many efforts towards building simulated environments for various tasks [6, 12, 40, 41, 42]. Much work has focused on indoor environments [6, 40, 42] based on public indoor datasets such as SUNCG [36] or Matterport3D [8]. In contrast to indoor settings where the environment is relatively simple and easy to model, simulators for autonomous driving exhibit significant challenges in modeling the complicated and dynamic scenarios of real-world scenes. TORCS[41] is one of the first simulation environments that support multi-agent racing, but is not tailored for real-world autonomous

driving research and development. DeepGTAV [1] provides a plugin that transforms the Grand Theft Auto gaming environment into a vision-based self-driving car research environment. CARLA[12] is a popular open-source simulation engine that supports the training and testing of SDVs. All these simulators rely on manual creation of synthetic environments, which is a formidable and laborious process. In CARLA [12], the 3D model of the environment, which includes buildings, road, vegetation, vehicles, and pedestrians, is manually created. The simulator provides one town with 2.9 km of drivable roads for training and another town with 1.4 km of drivable roads for testing. In contrast, our system is easily extendable to new scenes that are driven by an SDV. Furthermore, because the environment we are building is a high-quality reconstruction based on the vehicle sensors, it naturally closes the domain gap between synthetic and real contents, which is present in most traditional simulation environments. AADS [24] shares similar ideas as ours in that it also utilizes real sensor data to synthesize novel views. The major difference is that we reconstruct the 3D environment, while AADS uses a purely image-based novel view synthesis. Reconstructing the 3D environment gives us the freedom to synthesize novel views that could not be easily captured in the real world. Moreover, once our environment is built, we no longer need to store the images as well as the query of the nearest K views upon synthesis, which saves time for deployment.

Learning on Synthetic Data. Besides enabling end-to-end training and evaluation of embodied agents, the simulated environment can also provide a large amount of data for training deep neural networks. [33] uses a synthetic scene to generate a large amount of fully labeled training data for urban scene segmentation. [20] generate images containing

novel placement of dynamic objects to boost the performance of object detection.

Geometric Reconstruction and 3D Representations. Our work is also closely related to 3D reconstruction for outdoor environments. The typical approach is to use structure from motion [37, 39] and multi-view stereo [14] to recover a dense 3D point cloud from image collections, then optionally use Poisson reconstruction [22] to obtain a mesh representation. Such a paradigm is most suitable for the case where we have multiple images covering the same area from different perspectives, which is not always true in our case. Thanks to the rapid advancement of LiDAR technology, we can have accurate depth information to complement the camera image data. Our work uses this to augment the traditional surfel [32] representation with fine-grained image textures, which not only greatly simplifies the reconstruction process, but it also effectively enhances the representation of the colored real world. Truncated Signed Distance Functions [11] and their most recent variants [30] are also promising alternatives to the surfel. We also noted the recent work [3] that learns a point-wise dense descriptor on point cloud for rendering purpose. Although they’ve shown promising results, however their approach assumes a static environment, and is not practically applicable to outdoor scenario where a scene usually contains tens of millions of points.

GAN-based Image Translation. Generative Adversarial Networks (GAN) [15] have attracted broad interests in both academia and industry. While [15] aims at synthesis realistic images, [19] generalizes its framework to a more practical conditional image synthesis setting. Subsequent research [4, 21, 31, 44] has made great strides in improving the quality of images generated by GAN methods. We refer the readers to [10] for details on this topic. [38] trained a video synthesizer on Cityscape [9] that can convert video of a semantic map into a video of realistic images. However, their training procedure requires pixel-wise annotated semantic images, which is very expensive in practice. In contrast, our approach uses labeled 3D bounding boxes for several dynamic object classes and therefore is more cost-effective. We believe even this requirement can be further relaxed, by replacing the ground-truth 3D boxes with 3D boxes produced by a high-quality offline 3D perception pipeline. Finally, we address the usual problem of GAN evaluation by proposing two new metrics that are suitable for the task of novel view synthesis.

3. Approach

In this section, we explain the key innovations of this work, which lays the foundation for creating a data-driven simulation environment supporting sensor realism: surfel scene reconstruction and image synthesis via the SurfelGAN.

3.1. Surfel Scene Reconstruction

Enhanced Surfel Map. A good scene reconstruction should achieve faithful preservation of the sensor information while being efficient to compute and storage. We propose a novel texture-enhanced surfel map representation. Surfels are compact, easy to reconstruct, and because of their fixed size, easy to texture and compress. Below we describe our approach, which contains more fine-grained details compared to traditional surfel map representations [32].

We discretize the scene into a 3D voxel grid of fixed size and process LiDAR scans in the order they are captured. For each voxel, we construct a surfel disk by estimating the mean coordinate and the surfel normal, based on all the LiDAR points that fall within that voxel. The surfel disk radius is defined as $\sqrt{3}v$, where v denotes the voxel size. For the LiDAR points binned in a voxel, we also have corresponding colors from the camera image, which we can use to estimate the surfel color. Note that traditional surfel maps suffer from the trade-off between geometry consistency and fine-grained details, *i.e.*, a large voxel size gives better geometry consistency but fewer details, while small voxel size results in finer details but less stable geometry. Therefore, we take an alternative approach that aims to achieve both good geometry consistency and rich texture details. Specifically, we discretize each surfel disk into a $k \times k$ grid centered on its point centroid, as illustrated in subfigure b) in Fig. 1. Each grid center is assigned an independent color to encode higher-resolution texture details.

Since each surfel may have a different appearance across different frames, due to the variations of the lighting conditions and the changes of relative pose (distance and view angle), we propose to enhance the surfel representation by creating a codebook of such $k \times k$ grids at n various distances. For each bin, we determine its color from the first observation, which we found is important to obtain a smooth rendering image. During the rendering stage, we determine which $k \times k$ patch to use based on the camera pose. The final rendering is shown in Fig. 2. We can see that the baseline surfel map introduces many artifacts at object boundaries and yields non-smooth coloring at non-boundary areas. In contrast, our texture-enhanced surfel map eliminates much of the artifacts and gives vivid-looking images. In our experiments, we use $v = 0.2m$, $k = 5$ and $n = 10$.

Handling Dynamic Objects. We consider vehicles as rigid dynamic objects and reconstruct a separate model for each. For simplicity, we leverage the high-quality 3D bounding box annotations from the Waymo Open Dataset [2] to accumulate the LiDAR points from multiple scans for each object of interest. We apply the Iterative Closest Point (ICP) [34] algorithm to refine the point cloud registration, producing a dense point cloud that allows an accurate, enhanced surfel reconstruction for each vehicle. Please see Supplementary



Figure 2. Visualization of different scene modeling strategies. **Top row**: Surfel baseline; **Center row**: our Texture-Enhanced Surfel Map (also known as *surfel rendering* in the rest of the paper); **Bottom row**: Real camera image.

Sec. A for reconstructed examples. Our approach does not strictly require 3D box ground-truth; we could also leverage a state of the art vehicle detection and tracking algorithm [28, 35] to get initial estimates for ICP. However, we leave this experiment for future work.

When simulating our environment, the reconstructed vehicle models can be placed in any location of choice. In the case of the pedestrians, which are deformable objects, we reconstruct a separate surfel model for each LiDAR scan separately. We allow placement of the reconstructed pedestrian anywhere in the scene for that scan. We leave the task of accurate deformable model reconstruction from multiple scans to future work.

3.2. Image Synthesis via SurfelGAN

While the surfel scene reconstruction captures a rich environment representation, it produces surfel renderings that have a non-negligible realism gap when compared to real images, due to incomplete reconstruction and imperfect geometry and texturing (see Fig. 2). SurfelGAN is designed to address the issue.

Ultimately, we like to learn a generator (SurfelGAN) that converts surfel renderings rendered from the surfel scene reconstruction to realistically looking images. We treat semantic and instance segmentation maps as part of the surfel rendering. For the sake of simplicity, we omit to mention them explicitly.

Let the generator $G_{\theta_S}^{S \rightarrow I}$ be an encoder-decoder model parameterized by the learnable variable θ_S . Given pairs of surfel renderings \mathcal{S}_p and images \mathcal{I}_p , the supervised loss can be applied to train the generator. We call SurfelGAN that is trained solely with supervised learning **SurfelGAN-S**.

Additionally, We can add an adversarial loss dictated by a real image discriminator $D_{\phi_I}^I$ parameterized by trainable variable ϕ_I . SurfelGANs trained with this additional loss is named **SurfelGAN-SA**.

However, paired training data between surfel rendering and real image is very limited. Unpaired data is however easy to obtain. We leverage unpaired data for two purposes, *i.e.* improving the generalization of discriminator by training with more unlabeled examples, and regularizing the generator by enforcing cycle consistency. Let the reverse generator $G_{\theta_I}^{I \rightarrow S}$ be another encoder-decoder model which has the same architecture as $G_{\theta_S}^{S \rightarrow I}$ except more output channels for semantic/instance map, *any* surfel rendering, paired \mathcal{S}_p or unpaired \mathcal{S}_u can be translated to a real image and translated back to a surfel rendering, where a cycle consistency loss can be applied. The same applies to *any* paired \mathcal{I}_p or unpaired \mathcal{I}_u real image as well. Finally, we add the surfel rendering discriminator $D_{\phi_S}^S$ that judges generated surfel images. We call SurfelGANs trained with additional cycle consistency **SurfelGAN-SAC**. An intuitive overview of the training strategy is shown in Fig. 3. And please refer to Sec. 4 for a detailed description of paired and unpaired data. We optimize the following objective:

$$\begin{aligned}
 \max_{\phi_S, \phi_I} \min_{\theta_S, \theta_I} & \mathcal{L}_r(G_{\theta_S}^{S \rightarrow I}, \mathcal{S}_p, \mathcal{I}_p) + \lambda_1 \mathcal{L}_r(G_{\theta_I}^{I \rightarrow S}, \mathcal{I}_p, \mathcal{S}_p) \\
 & + \lambda_2 \mathcal{L}_a(G_{\theta_S}^{S \rightarrow I}, D_{\phi_I}^I, \mathcal{S}_{p,u}) + \lambda_3 \mathcal{L}_a(G_{\theta_I}^{I \rightarrow S}, D_{\phi_S}^S, \mathcal{I}_{p,u}) \\
 & + \lambda_4 \mathcal{L}_c(G_{\theta_S}^{S \rightarrow I}, G_{\theta_I}^{I \rightarrow S}, \mathcal{S}_{p,u}) + \lambda_5 \mathcal{L}_c(G_{\theta_I}^{I \rightarrow S}, G_{\theta_S}^{S \rightarrow I}, \mathcal{I}_{p,u})
 \end{aligned} \tag{1}$$

where \mathcal{L}_r , \mathcal{L}_a , \mathcal{L}_c are supervised reconstruction, adversarial, and cycle consistency loss. We use hinged Wasserstein loss for adversarial training [25, 29, 43] in our experiments as it

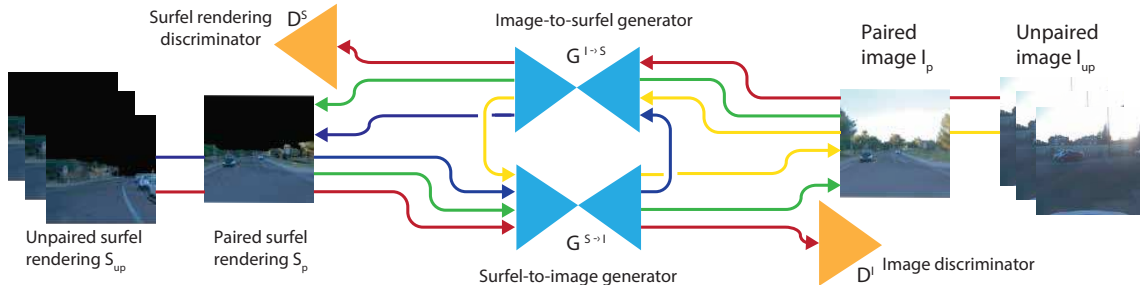


Figure 3. (Best viewed in color) **SurfelGAN training paradigm.** The training setup has two symmetric encoder-decoder generators mapping from surfel renderings to real images $G^{S \rightarrow I}$ and vice versa $G^{I \rightarrow S}$. Additionally, there are two discriminators, D^S , D^I , which specialize in the surfel and the real domain. The losses are shown as colored arrows. Green: supervised reconstruction loss. Red: adversarial loss. Blue/Yellow: cycle-consistency losses. When training with paired data, e.g. WOD-TRAIN, the surfel renderings translate to real images, and we can apply a one-directional supervised reconstruction loss (SurfelGAN-S) only or add an additional adversarial loss (SurfelGAN-SA). When training with unpaired data, we can go either from the surfel renderings (e.g. WOD-TRAIN-NV) or the real images (e.g. Internal Camera Dataset), use one of the encoder-decoder networks to get to the other domain and back. We can then apply a cycle consistency loss. (SurfelGAN-SAC). The encoder-decoder networks consist of 8 convolutional and 8 deconvolutional layers. Discriminators consist of 5 convolutional layers. All network operate on 256×256 sized input.

helps to stabilize the training. We use ℓ^1 -loss as reconstruction and cycle-consistency loss for renderings and images and cross entropy loss for semantic and instance maps.

Distance Weighted Loss. Due to the limited coverage of the surfel map, our surfel rendering contains large areas of unknown regions. The uncertainty in those regions is much higher than that of the region with surfel information. Also, the distance between the camera and the surfel introduces another factor of uncertainty. Therefore, we use a distance weighted loss to stabilize our GAN training. Specifically, during data pre-processing, we generate a distance map that records the nearest distance to the observed region and then uses the distance information as weighting coefficients to modulate our reconstruction loss.

Training Details. We use Adam[23] optimizer for training. We set the initial learning rate to $2e-4$ for both the generator and the discriminator and set $\beta_1 = 0.5$ and $\beta_2 = 0.9$. We use batch normalization [18] after Relu activation. We set $\lambda_1 = 1$, $\lambda_2, \lambda_3 = 0.001$, $\lambda_4, \lambda_5 = 0.1$ in all of our experiments. The total training time of our network is 3 days, based on one Nvidia Titan V100 GPU with batch size 8.

4. Experimental Results

We base our experiments mainly on the Waymo Open Dataset [2], but we also collected two additional datasets to support our experiments further.

Waymo Open Dataset (WOD) [2]. The dataset consists of 798 training (WOD-TRAIN) and 202 validation (WOD-EVAL) sequences. Each sequence contains 20 seconds of camera and LiDAR data captured at 10Hz, as well as fully annotated 3D bounding boxes for vehicles, pedestrians, and cyclists. The LiDAR data covers a full 360 degrees around the agent, whereas five cameras capture the frontal 180 degrees. After reconstructing the surfel scenes, we can render

the surfel images in the same pose as the original camera images, hence generating surfel-image-to-camera-image pairs that can be used for paired training and evaluation. Since during the reconstruction process we know the category for each surfel, we can easily derive both semantic segmentation mask and instance segmentation mask by first rendering an index map that associates each pixel with a surfel index and then determine the semantic class or instance number through a look-up table.

We derive another dataset from WOD, which we call Waymo Open Dataset-Novel View (WOD-TRAIN-NV and WOD-EVAL-NV). We again start from reconstructed surfel scenes, but we now render surfel images from novel camera poses perturbed from existing camera poses. The perturbation consists of applying a random translation and a random yaw angle perturbation to the camera mounted vehicle. We use annotated 3D bounding boxes to ensure the perturbed vehicle does not intersect with others.

We generate one new surfel image rendering for each frame in the original dataset. Noted that although this dataset comes for free, i.e. we could generate any number of testing frames, it does not have corresponding camera images. Therefore, this dataset can only be used for unpaired training and not all types of evaluation paradigms.

Internal Camera Image Dataset. We collected additional 9.8k short sequences (100 frames for each) similar to WOD images. These unannotated images are used for unpaired training of real images.

Dual-Camera-Pose Dataset (DCP) Finally, we built a unique dataset tailored for measuring the realism of our model. The dataset contains scenarios where two vehicles observe the same scene at the same time. Specifically, we find the interval where two vehicles are within $20m$ of each other. We use the sensor data from the first vehicle to reconstruct the scene, and render the surfel image at the exact pose

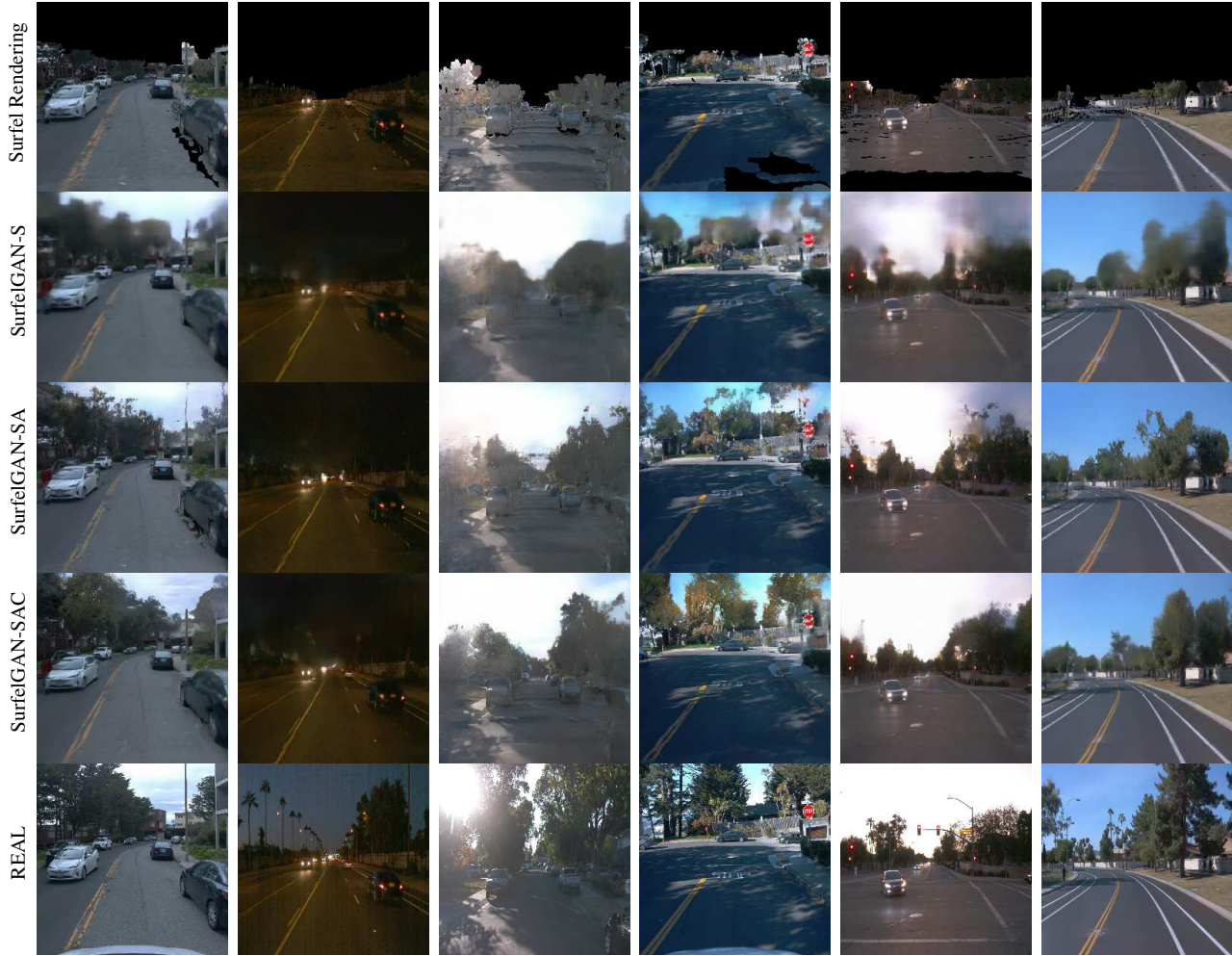


Figure 4. Qualitative comparison between different SurfElGAN variants and the baseline on WOD-EVAL under different weather conditions.

of the second vehicle. After filtering cases where the scene reconstruction is too incomplete, we obtain around 1k pairs, for which we can directly measure the pixel-wise accuracy of the generated image.

4.1. Model Variants and Baseline

Most experiments were performed on three variants of our proposed model. **Supervised (S)**: we train the surfel-rendering-to-image model in a supervised way by minimizing an ℓ^1 -loss between the generated image and the groundtruth real image. This type of training requires paired data. Hence, it is only possible to train on WOD-TRAIN. **Supervised + Adversarial (SA)**: we still only consider WOD-TRAIN as the training data. However, we add an adversarial loss alongside the ℓ^1 -loss. **Supervised + Adversarial + Cycle (SAC)**: in this variation, we also use WOD-TRAIN-NV and the Internal Camera Image Dataset. Since these two sets are unpaired, the supervised loss does not apply. We propose to use a cycle-consistency loss in addition to the adversarial loss, as discussed in Sec. 3.2.

The baseline for our applications is the direct surfel ren-

derings (**Surfel**) that serve as the input to our model.

4.2. Vehicle Detector Realism

Since the primary application of this work is the simulation of the camera data, a natural quality metric is to evaluate it using a downstream module. To this end, we like to know, without any fine-tuning, how well an off-the-shelf vehicle detector performs on the generated images, and, whether the detector perceived the generated images similarly to real images. We chose to use a vehicle detector with a ResNet architecture [17] and an SSD detection head [27], trained and evaluated on resized images of a 512×512 resolution. It is trained on a mixture of datasets that include WOD-TRAIN.

We trained our SurfElGAN model variants on a mixture of WOD-TRAIN, WOD-TRAIN-NV, and the Internal Camera Image Dataset, and generated images on WOD-TRAIN-NV, WOD-EVAL and WOD-EVAL-NV. Tab. 1 shows the quantitative comparison of the detector’s quality on the original surfel renderings that is the input SurfElGAN, images generated from the variants of SurfElGAN and real images. A few examples are displayed in Fig. 4. Please find additional visu-

	WOD-TRAIN-NV				WOD-EVAL				WOD-EVAL-NV			
	AP@50 ↑	AP@75 ↑	AP ↑	Rec ↑	AP@50	AP@75	AP	Rec	AP@50	AP@75	AP	Rec
Surfel (baseline)	0.444	0.168	0.211	0.342	0.521	0.168	0.239	0.371	0.462	0.154	0.213	0.348
SurfelGAN-S (ours)	0.508	0.177	0.236	0.359	0.576	0.164	0.252	0.341	0.514	0.159	0.230	0.358
SurfelGAN-SA (ours)	0.554	0.200	0.259	0.382	0.610	0.174	0.266	0.394	0.567	0.180	0.257	0.387
SurfelGAN-SAC (ours)	0.564	0.200	0.263	0.385	0.620	0.181	0.272	0.400	0.570	0.181	0.258	0.388
Real (upper bound)	-	-	-	-	0.619	0.198	0.281	0.424	-	-	-	-

Table 1. realism w.r.t. an off-the-shelf vehicle object detector. We generated images using the proposed SurfelGAN and ran inference on them using an off-the-shelf object detector. We report the standard COCO object detection metrics [26], including variants of the average-precision (AP) and recall at 100 (Rec). **Surfel** is the surfel rendering that is the input to SurfelGAN. **SurfelGAN** is the proposed model. The S variant is trained with paired supervised learning only. The SA variant adds the adversarial loss, and the SAC variant makes use of additional unpaired data and applied a cyclic adversarial loss. **Real** is the real image captured by cameras, which is only available in WOD-EVAL. It serves as an upper bound to the detector’s quality. As shown above, SurfelGAN significantly improves over the baseline, and reaches competitive quality metric values as the real images.

alizations in the supplementary material. Fig. 5 highlights our system’s ability to generate images in novel views.

It is notable that our texture-enhanced surfel scene reconstruction already produces surfel renderings that achieve good detection quality on the WOD-EVAL set at 52.1% AP@50. But there is still a significant gap between these surfel renderings and real images at 61.9%, which motivates our SurfelGAN work. As shown in Tab. 1, SurfelGAN-S, -SA and -SAC variants gradually improve over the baseline surfel renderings. SurfelGAN-SAC ultimately improves the AP@50 metric from 52.1% to 62.0% on WOD-EVAL, which is on par to the real images at 61.9%. It shows that images generated by SurfelGAN-SAC are close to real images in the eyes of the detector, which is the primary motivation of this work.

There are two types of generalization worth discussing. The first type is whether a SurfelGAN model trained on one set of scenes (*e.g.* WOD-TRAIN and WOD-TRAIN-NV) generalizes to new scenes (*e.g.* WOD-EVAL and WOD-EVAL-NV). We believe that the SurfelGAN model generalizes well since the relative improvement of SurfelGAN over the baseline is very similar between the WOD-TRAIN-NV and WOD-EVAL-NV columns in Tab. 1.

The second type of generalization is whether surfel rendering has a strong bias towards the poses from which the scene was reconstructed. We compare the metric values between WOD-EVAL and WOD-EVAL-NV. Although SurfelGAN improved by roughly 10% over the baseline in both cases, there is a noticeable quality difference between the two columns. To better understand this difference, in Tab. 2, we breakdown the metrics of SurfelGAN-SAC on WOD-EVAL-NV according to how much each pose deviates from the original poses in WOD-EVAL. The deviation $d(\cdot)$ is defined as a weighted sum of both translational and rotational differences of the poses:

$$d((t, R), (t', R')) = \|t - t'\| + \lambda_R \frac{\|\log(R^T R')\|}{\sqrt{2}} \quad (2)$$

where t and R are the pose (translation and rotation) of the

Perturbation	AP@50	AP@75	AP
$d \leq 1.0$	0.574	0.174	0.257
$1.0 < d \leq 2.0$	0.547	0.173	0.246
$2.0 < d$	0.488	0.153	0.218

Table 2. Detector metric break down at different perturbation level on WOD-EVAL-NV.

	Surfel	SGAN-S	SGAN-SA	SGAN-SAC
ℓ^1 -distance ↓	0.262	0.229	0.240	0.238

Table 3. Image-pixel realism. We applied the SurfelGAN on the Dual-Camera-Pose Dataset, where it is possible to measure ℓ^1 -distance error between the generated images and the real ones.

novel view in WOD-EVAL-NV, and t' , R' the pose of its closest pose in WOD-EVAL. λ_R is chosen to be 1.0.

It is an indication that the surfel renderings do have a quality bias w.r.t viewing direction, which means we should not perturb too much from the original poses if we want higher quality synthesized data. However, we believe that this problem can be negated if we were to reconstruct the surfel scene from multiple runs which bring in more accuracy. We did not explore this direction but left it to future work.

4.3. Image-Pixels Realism

The Dual-Camera-Pose (DCP) Dataset contains scenarios where two vehicles observe the same scene at the same time so that we can reconstruct the surfel scene using one camera and generate images at the poses of the second camera. We then match the generated image to the real one and report the ℓ^1 -distance error on the pixels that are covered by the surfel rendering. This is to ensure that there is a fair comparison between the surfel renderings and the generated images. Like in the previous experiment, the model is trained using WOD-TRAIN, WOD-TRAIN-NV, and the Internal Camera Image Dataset. The results are showing in Tab. 3. SurfelGAN improves on top of the surfel renderings, generating images that are closer to real images in ℓ^1 -distance. However, it is worth noting that the SurfelGAN-S version outperforms



Figure 5. Novel View Synthesis. The first column is Surfel image under novel view, the second column is our synthesized result. The third column is the original view. Additional visualization can be found in Supplementary Sec. B.

both SA and SAC that used additional losses and data during training. This finding is not unexpected since SurfelGAN-S optimizes for the ℓ^1 -distance.

4.4. Improving Detection by Data Augmentation

In a bonus experiment, we explore whether the generated images are helpful as a tool of data augmentation to training a vehicle object detector. For the baseline, we trained a vehicle detector on WOD-TRAIN and evaluated the detector’s quality on WOD-EVAL. We then trained another vehicle detector using both WOD-TRAIN and surfel images generated from WOD-TRAIN-NV, and also evaluated on WOD-EVAL.

WOD-TRAIN-NV only inherits 3D bounding boxes from WOD-TRAIN, and does not contain tightly fitting 2D bounding boxes like those in WOD-TRAIN. We approximate the latter by projecting all surfels in the 3D bounding boxes to the 2D novel view and take the axis-aligned bounding box as an approximation. The results are shown in Tab. 4. The data augmentation significantly boosted the detector’s metric on average precision, boosting the AP@50 score from 21.9% to 25.4%, the AP@75 from 10.8% to 12.1%, and the average AP from 11.9% to 13.0%. It is worth noting that these AP scores are much lower than those in Tab. 1. The main reason for the discrepancy is that images are resized differently in order to use the off-the-shelf detector in Tab. 1. We also trained on surfel renderings directly. There is a slight improvement compared to training only on WOD-TRAIN. But there is still a significant gap between augmenting using SurfelGAN synthesized images, which further demonstrate the realism of the SurfelGAN model.

4.5. Limitations

The surfel scene reconstruction has its limitations. The surfel scene reconstruction might fail to reconstruct certain areas of the scene, as illustrated in the top row in Fig. 6.

Training Set	AP@50	AP@75	AP
WOD-TRAIN	0.219	0.108	0.119
+ WOD-TRAIN-NV Surfel	0.228	0.111	0.120
+ WOD-TRAIN-NV SurfelGAN	0.254	0.121	0.130

Table 4. Detector metric on Open Dataset validation set when trained with different combination of data.



Figure 6. We show two typical failure cases, the first is the case where reconstructed Surfel map contains too large errors. The second is on the unmapped region (top part of building in this example).

In this particular case, SurfelGAN was unable to recover from broken geometry, resulting in an unrealistically looking vehicle. Another case is at the place where the surfel map does not cover. Lacking any surfel cues forces the model’s output to have a high variance, especially when it tries to hallucinate patterns that infrequently appear in the dataset, such as tall buildings. This observation suggests rooms for improvement in the reconstruction stage. In the case where we only have partial geometry, applying a learned geometry completion model first could be more helpful than relying solely on the generating module to resolve all artifacts.

5. Conclusion

In this work, we proposed a simple yet effective data-driven approach, which can synthesize camera data for autonomous driving simulations. Based on camera and lidar data captured by a vehicle pass through a scene, we reconstruct a 3D model using our Enhanced Surfel Map representation. Given this representation, we are able to render novel views and configurations of objects in the environment. We use our SurfelGAN image synthesis model to fix any reconstruction, occlusion or rendering artifacts. To the best of our knowledge, we have built the first purely data-driven camera simulation system for autonomous driving. Experimental results not only demonstrate the high level of realism of our synthesized sensor data, but also show the data can be used for training dataset augmentation for deep neural networks. In future work, we plan to enhance camera simulation further by improving the dynamic object modeling process and by investigating temporally consistent synthesis module.

References

- [1] Deepgtav v2. [2](#)
- [2] Waymo open dataset: An autonomous driving dataset, 2019. [3](#), [5](#)
- [3] Kara-Ali Aliiev, Dmitry Ulyanov, and Victor Lempitsky. Neural point-based graphics. *arXiv preprint arXiv:1906.08240*, 2019. [3](#)
- [4] Martin Arjovsky, Soumith Chintala, and Léon Bottou. Wasserstein gan. *arXiv preprint arXiv:1701.07875*, 2017. [3](#)
- [5] Mayank Bansal, Alex Krizhevsky, and Abhijit Ogale. Chauffeurnet: Learning to drive by imitating the best and synthesizing the worst. In *RSS*, 2019. [1](#)
- [6] Simon Brodeur, Ethan Perez, Ankesh Anand, Florian Golemo, Luca Celotti, Florian Strub, Jean Rouat, Hugo Larochelle, and Aaron Courville. Home: A household multimodal environment. *arXiv preprint arXiv:1711.11017*, 2017. [2](#)
- [7] Yuning Chai, Benjamin Sapp, Mayank Bansal, and Dragomir Anguelov. Multipath: Multiple probabilistic anchor trajectory hypotheses for behavior prediction. *arXiv preprint arXiv:1910.05449*, 2019. [1](#)
- [8] Angel Chang, Angela Dai, Thomas Funkhouser, Maciej Halber, Matthias Niessner, Manolis Savva, Shuran Song, Andy Zeng, and Yinda Zhang. Matterport3d: Learning from rgb-d data in indoor environments. *arXiv preprint arXiv:1709.06158*, 2017. [2](#)
- [9] Marius Cordts, Mohamed Omran, Sebastian Ramos, Timo Rehfeld, Markus Enzweiler, Rodrigo Benenson, Uwe Franke, Stefan Roth, and Bernt Schiele. The cityscapes dataset for semantic urban scene understanding. In *CVPR*, 2016. [3](#)
- [10] Antonia Creswell, Tom White, Vincent Dumoulin, Kai Arulkumaran, Biswa Sengupta, and Anil A Bharath. Generative adversarial networks: An overview. *IEEE Signal Processing Magazine*, 2018. [3](#)
- [11] Brian Curless and Marc Levoy. A volumetric method for building complex models from range images. In *Proceedings of the 23rd Annual Conference on Computer Graphics and Interactive Techniques*, SIGGRAPH '96, 1996. [3](#)
- [12] Alexey Dosovitskiy, German Ros, Felipe Codevilla, Antonio Lopez, and Vladlen Koltun. Carla: An open urban driving simulator. *arXiv preprint arXiv:1711.03938*, 2017. [1](#), [2](#)
- [13] Michael Everett, Yu Fan Chen, and Jonathan P How. Motion planning among dynamic, decision-making agents with deep reinforcement learning. In *IROS*, 2018. [1](#)
- [14] Yasutaka Furukawa and Jean Ponce. Accurate, dense, and robust multi-view stereopsis. *TPAMI*, 2010. [3](#)
- [15] Ian Goodfellow, Jean Pouget-Abadie, Mehdi Mirza, Bing Xu, David Warde-Farley, Sherjil Ozair, Aaron Courville, and Yoshua Bengio. Generative adversarial nets. In *NeurIPS*, 2014. [2](#), [3](#)
- [16] Kaiming He, Georgia Gkioxari, Piotr Dollár, and Ross Girshick. Mask r-cnn. In *ICCV*, 2017. [1](#)
- [17] Kaiming He, Xiangyu Zhang, Shaoqing Ren, and Jian Sun. Deep residual learning for image recognition. In *CVPR*, 2016. [6](#)
- [18] Sergey Ioffe and Christian Szegedy. Batch normalization: Accelerating deep network training by reducing internal covariate shift. *arXiv preprint arXiv:1502.03167*, 2015. [5](#)
- [19] Phillip Isola, Jun-Yan Zhu, Tinghui Zhou, and Alexei A Efros. Image-to-image translation with conditional adversarial networks. In *CVPR*, 2017. [3](#)
- [20] Amlan Kar, Aayush Prakash, Ming-Yu Liu, Eric Cameracci, Justin Yuan, Matt Rusiniak, David Acuna, Antonio Torralba, and Sanja Fidler. Meta-sim: Learning to generate synthetic datasets. *arXiv preprint arXiv:1904.11621*, 2019. [2](#)
- [21] Tero Karras, Timo Aila, Samuli Laine, and Jaakko Lehtinen. Progressive growing of gans for improved quality, stability, and variation. *arXiv preprint arXiv:1710.10196*, 2017. [3](#)
- [22] Michael Kazhdan, Matthew Bolitho, and Hugues Hoppe. Poisson surface reconstruction. In *Proceedings of the fourth Eurographics symposium on Geometry processing*, volume 7, 2006. [3](#)
- [23] Diederik P Kingma and Jimmy Ba. Adam: A method for stochastic optimization. *arXiv preprint arXiv:1412.6980*, 2014. [5](#)
- [24] Wei Li, Chengwei Pan, Rong Zhang, Jiaping Ren, Yuxin Ma, Jin Fang, Feilong Yan, Qichuan Geng, Xinyu Huang, Huajun Gong, et al. Aads: Augmented autonomous driving simulation using data-driven algorithms. *arXiv preprint arXiv:1901.07849*, 2019. [2](#)
- [25] Jae Hyun Lim and Jong Chul Ye. Geometric gan. *arXiv preprint arXiv:1705.02894*, 2017. [4](#)
- [26] Tsung-Yi Lin, Michael Maire, Serge J. Belongie, James Hays, Pietro Perona, Deva Ramanan, Piotr Dollár, and C. Lawrence Zitnick. Microsoft COCO: common objects in context. In *ECCV*, 2014. [7](#)
- [27] Wei Liu, Dragomir Anguelov, Dumitru Erhan, Christian Szegedy, Scott Reed, Cheng-Yang Fu, and Alexander C Berg. Ssd: Single shot multibox detector. In *ECCV*, pages 21–37. Springer, 2016. [1](#), [6](#)
- [28] Wenjie Luo, Bin Yang, and Raquel Urtasun. Fast and furious: Real time end-to-end 3d detection, tracking and motion forecasting with a single convolutional net. In *CVPR*, 2018. [4](#)
- [29] Takeru Miyato, Toshiki Kataoka, Masanori Koyama, and Yuichi Yoshida. Spectral normalization for generative adversarial networks. *arXiv preprint arXiv:1802.05957*, 2018. [4](#)
- [30] Jeong Joon Park, Peter Florence, Julian Straub, Richard Newcombe, and Steven Lovegrove. Deepsdf: Learning continuous signed distance functions for shape representation. In *CVPR*, 2019. [3](#)
- [31] Taesung Park, Ming-Yu Liu, Ting-Chun Wang, and Jun-Yan Zhu. Semantic image synthesis with spatially-adaptive normalization. In *CVPR*, 2019. [3](#)
- [32] Hanspeter Pfister, Matthias Zwicker, Jeroen Van Baar, and Markus Gross. Surfels: Surface elements as rendering primitives. In *Proceedings of the 27th annual conference on Computer graphics and interactive techniques*, 2000. [3](#)
- [33] German Ros, Laura Sellart, Joanna Materzynska, David Vazquez, and Antonio M Lopez. The synthia dataset: A large collection of synthetic images for semantic segmentation of urban scenes. In *CVPR*, 2016. [2](#)
- [34] A. Segal, D. Haehnel, and S. Thrun. Generalized-icp. In *Proceedings of Robotics: Science and Systems*, 2009. [3](#)

- [35] Shaoshuai Shi, Zhe Wang, Xiaogang Wang, and Hongsheng Li. Part-a² net: 3d part-aware and aggregation neural network for object detection from point cloud. *arXiv preprint arXiv:1907.03670*, 2019. 4
- [36] Shuran Song, Fisher Yu, Andy Zeng, Angel X Chang, Manolis Savva, and Thomas Funkhouser. Semantic scene completion from a single depth image. In *CVPR*, 2017. 2
- [37] Shimon Ullman. The interpretation of structure from motion. *Proceedings of the Royal Society of London. Series B. Biological Sciences*, 1979. 3
- [38] Ting-Chun Wang, Ming-Yu Liu, Jun-Yan Zhu, Guilin Liu, Andrew Tao, Jan Kautz, and Bryan Catanzaro. Video-to-video synthesis. *arXiv preprint arXiv:1808.06601*, 2018. 3
- [39] Changchang Wu et al. Visualsfm: A visual structure from motion system. 2011. 3
- [40] Yi Wu, Yuxin Wu, Georgia Gkioxari, and Yuandong Tian. Building generalizable agents with a realistic and rich 3d environment. *arXiv preprint arXiv:1801.02209*, 2018. 2
- [41] Bernhard Wymann, Eric Espié, Christophe Guionneau, Christos Dimitrakakis, Rémi Coulom, and Andrew Sumner. Torcs, the open racing car simulator. *Software available at <http://torcs.sourceforge.net>*, 2000. 2
- [42] Fei Xia, Amir R Zamir, Zhiyang He, Alexander Sax, Jitendra Malik, and Silvio Savarese. Gibson env: Real-world perception for embodied agents. In *CVPR*, 2018. 2
- [43] Han Zhang, Ian Goodfellow, Dimitris Metaxas, and Augustus Odena. Self-attention generative adversarial networks. *arXiv preprint arXiv:1805.08318*, 2018. 4
- [44] Jun-Yan Zhu, Taesung Park, Phillip Isola, and Alexei A Efros. Unpaired image-to-image translation using cycle-consistent adversarial networks. In *ICCV*, 2017. 3